

Article

Numerical Investigation of Mixing Characteristic for CH₄/Air in Rotating Detonation Combustor

Shan Jin, Qingyang Meng, Zhiming Li *, Ningbo Zhao *, Hongtao Zheng and Jialong Yang

College of Power and Energy Engineering, Harbin Engineering University, Harbin 150001, China; jinshan512@hrbeu.edu.cn (S.J.); mengqingyang@hrbeu.edu.cn (Q.M.); zhenghongtao9000@163.com (H.Z.); yangjialong@hrbeu.edu.cn (J.Y.)

* Correspondence: cruyff@hrbeu.edu.cn (Z.L.); zhaoningbo314@hrbeu.edu.cn (N.Z.)

Received: 25 December 2019; Accepted: 12 February 2020; Published: 14 February 2020



Abstract: The mixing process of fuel and oxidizer is a very critical factor affecting the real operating performance of non-premixed rotating detonation combustor. In this paper, a two-dimensional numerical study is carried out to investigate the flow and mixing characteristics of CH₄/air in combustor with different injection structures. On this basis, the effect of CH₄/air mixing on the critical ignition energy for forming detonation is theoretically analyzed in detail. The numerical results indicate that injection strategies of CH₄ and air can obviously affect the flow field characteristic, pressure loss, mixing uniformity and local equivalence ratio in combustor, which further affect the critical ignition energy for forming detonation. In the study for three different mass flow rates (the mass flow rates of air are 12.01 kg/s, 8.58 kg/s and 1.72 kg/s, respectively), when air is radially injected into combustor (fuel/air are injected perpendicular to each other), although the mixing quality of CH₄ and air is improved, the total pressure loss is also increased. In addition, the comparative analysis also shows that the increase of mass flow rate of CH₄/air can decrease the difference of the critical ignition energy for forming detonation at a constant total equivalence ratio. The ignition energy decreases with the decrease of the total flow rate and then increases gradually.

Keywords: rotating detonation; numerical simulation; mixing characteristic; equivalence ratio; flow field characteristic

1. Introduction

Detonation is a supersonic combustion process relating to pressure gain from reactants to products and has lower emission of the nitrogen oxides (NO_x), which becomes the major motivation for researchers to actively investigate the detonation-based propulsion device [1]. Detonation theoretically consists of the leading shock wave and a reaction zone compactly following it [2,3]. Compared with deflagration, detonation has faster reactive rate, lower entropy production and nitrogen oxides (NO_x) emission [4,5]. Besides, the method to optimize the deflagration-based combustor seems to encounter its limit in recent years. In view of the above considerations, developing detonation-based combustor is a reasonable approach to promote propulsion device entering a new stage. In the past 20 years, a considerable number of investigations were carried out on detonation-based combustor using different formations of detonation wave. The main detonation-based engines include rotating detonation engine (RDE) [6–8], pulsed detonation engine (PDE) [9–11] and standing oblique detonation engine (ODE) [12,13]. In recent years, PDE and RDE is more competitive compared to ODE and capture more researchers' attention consequently. Regarded as a potential pressure gain propulsive device, PDE has been deeply investigated in the past few decades and achieve a lot of promising progress. However, the expectation of using PDE to replace traditional deflagration-based engine has to be diminished due to the complex operational process of PDE. The working process of PDE refers to periodic gas inflation,

repeating ignition, and exhaustion, which results in its working frequency is limited on the order of approximately hundreds of Hertz. On the contrary to PDE, the reactant in RDE is injected into the combustor continuously and this can negate the disadvantages of complicated working process such as PDE. After once ignition, the rotating detonation wave (RDW) propagates ceaselessly in rotating detonation combustor (RDC) consuming fresh reactant injected from the head-end inlet simultaneously. Therefore, the working frequency of RDE reaches on the order of thousands of Hertz far higher than PDE. Such high frequency and continuous propagation of detonation wave guarantee the stable thrust output on the outlet. Even though RDE avoids the gas inflation and exhaustion process, proper injection condition and inlet structure are key factors of stable propagation for RDW.

The formation and stable propagation of RDW are strongly dependent on the injection condition. Local reactant injected from the plenum will be blocked by RDW due to its high pressure behind the leading shock wave [14–16]. The reactant intake depends on the local pressure in combustor and the inflow cannot recover until RDW skims over. If the blocking time of reactant is too long, RDW might extinguish in the next period due to lack of enough fresh reactant supporting the energy for RDW. To avoid the extinguishment phenomenon occurring in combustor, high injection pressure is preferred because it can recover reactant intake earlier and provide fresh reactant in time for RDW. However, over high injection pressure will increase the injection velocity of reactant, which may cause the RDW transform into standing detonation wave [17].

The injection scheme of RDC can be divided into two types, namely premixed injection, and non-premixed injection. To gain stable and well-organized RDW, the premixed injection scheme is employed in most of numerical simulations. Nevertheless, the premixed injection scheme cannot describe and capture the mixing process of fuel and oxidizer during the operation of RDC, which deviates from the real process of the experiment. Besides, the premixed injection scheme has the risk of flashback because of the high activity of premixed reactant in inlet holes or slot. On this account, the non-premixed injection scheme is applied to the majority of experiments. Due to the non-premixed injection involved in the mixing process and the mixing time being extremely transient because of the short period of RDW propagation in the combustor, it is difficult to achieve the ideal mixing degree for fuel and oxidizer as premixed injection does. As a result, the mixture of fuel and oxidizer is non-homogenous in the fresh gas layer ahead of detonation wave, which makes the RDW structure is not as distinct as that of premixed injection condition and the stability of RDW is also weakened correspondingly. To minimize the above weakness of non-premixed injection in RDC, two significant problems have to be solved: (1) how to make fuel and oxidizer mix sufficiently and rapidly in limited space, (2) how to minimize the pressure loss during mixing process so as to guarantee the performance of RDC.

Using H_2 /air as reactant, Frolov et al. [18] numerically investigated three-dimensional RDW with non-premixed injection and compared the parameters of RDW with experimental data. The numerical results indicated that the fresh reactant height in front of RDW is approximately 100 mm~150 mm under their calculated condition, which was favorable according to experimental measurement data [19]. Standard et al. [20,21] simplified the cylindrical RDC into cuboid-shaped combustor and conducted three-dimensional simulation to explore the mixing characteristics of H_2 and air in combustor with different inlet structures. They thought that fuel injected by multiple holes was benefit for increasing mixing quality for hole/slot injection scheme. Taking H_2 and air mass flow rate, H_2 injection position and back pressure on the outlet into account, Driscoll et al. [22,23] investigated the effect of different factors on mixing characteristics in RDC. The results revealed that moving the H_2 injecting position into air intake slot and increasing back pressure would enhance the mixing efficiency and quality. Besides, they pointed out that the number of H_2 injecting holes exist at an optimum value which made the H_2 and air mixing quality be the best when the air injecting area is kept constant. By means of Large Eddy Simulation (LES), Gaillard et al. [24] numerically investigated an injection element of RDC to study H_2/O_2 mixing characteristic expecting to reflect the whole mixing situation of RDC. They believed that shear force and collision effect must be taken into account for inlet structure design of combustor to achieve the favorable mixing performance. Ionio Q et al. [25] firstly reported the

successful air-breathing premixed RDE. The premixed flow maintained a boundary layer velocity gradient that successfully arrested flashback. Then, they showed the design principles of quenching distance and critical boundary layer velocity gradients and described the safe operation region for a premixed RDE when adjusted for experimental conditions and applied in unison [26].

Hydrogen was widely used in RDC experiments and numerical simulations due to its high detonability and calorific value compared to other fuels. However, as one of the most common fuels, CH₄ is little if anything chosen as the propellant in RDC. Considering CH₄ is abundant in nature, moderate detonability and low explosion hazard compared to H₂, it can possibly become the fuel for RDC in the future. However, one problem has to be faced which is that the critical ignition energy of CH₄ is much higher than H₂. Therefore, how to reduce the critical ignition energy of CH₄ is the first puzzle to be solved. It is well known that the optimum position for ignition is the spot where equivalence ratio is close to 1 in the combustor. This means that favorable mixing characteristic is crucial for successful ignition, and it is also a guarantee for stable propagation of RDW in the first period. Besides, lower loss of the total pressure will have finally some gain in total pressure on the combustor outlet. Different inlet structures of RDC affect the mixing quality and total pressure loss across the combustor simultaneously. Therefore, seeking a proper inlet structure of RDC is beneficial to make the CH₄ as the propellant of RDC possible.

In view of the above considerations, a parametric numerical investigation is carried out to explore the cold mixing characteristic and total pressure loss of CH₄ and air under different inlet structures. This study aims to compare flow field organization of different inlet structures and understand the total pressure variations during the mixing process. This article firstly studies the effects of different inlet structures on mixing characteristics. After that, the effects of inlet structures on the total pressure loss are analyzed. On this basis, the ignition energies of different inlet structures are also calculated.

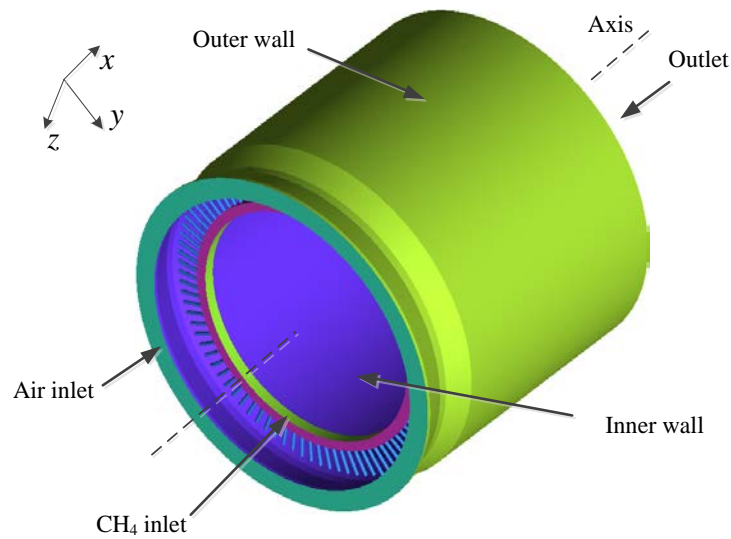
2. Numerical Model and Methods

2.1. Physical Model and Computational Domain

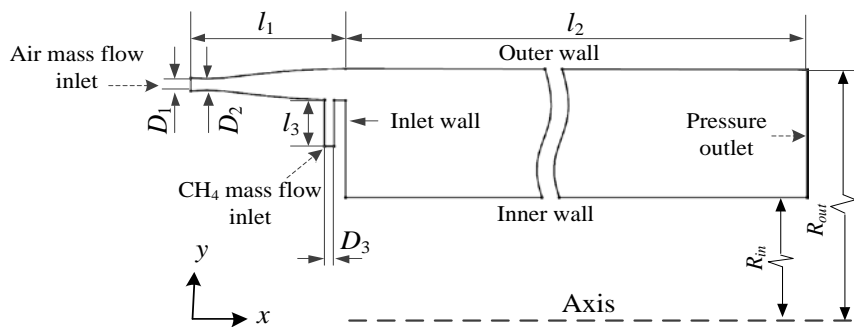
The schematic of RDC is shown in Figure 1. The RDC used in this paper is a coaxial ring type combustor with an inner diameter and outer diameter of 640 mm and 700 mm, respectively. The RDC consists of the inner wall, outer wall, air inlet and CH₄ inlet of the combustor. Figure 1a describes three-dimensional model of RDC, the two-dimensional cross section along axis is shown in Figure 1b. It is to be found in Figure 1 that air is injected by a Laval nozzle shaped slot, and CH₄ is injected through the holes evenly spaced on a circle of inner wall. Among them, there are 60 spray holes evenly distributed on the inner wall of the combustor. This paper mainly investigates the effect of fuel and air injection on mixing effect. Injector spacing is not in the scope of study. This article studies the effects of injection strategies on blending effects and does not consider the effects of injector interactions on fuel and air blending effects. Therefore, there is no need to perform three-dimensional numerical simulation on RDC. At the same time, Driscoll et al. [22] proposed that simplifying holes of fuel inlet into slot is accessible for cold mixing process study of RDC. Synthesizing the symmetry properties of combustor, Figure 1b was selected as the computational domain and x axis was set as symmetric axis. The geometry size of computational domain is listed in Table 1.

Table 1. Structure parameters of computational domain.

l_1/mm	l_2/mm	l_3/mm	D_1/mm
15.9	1000.0	5.0	1.4
D_2/mm	D_3/mm	R_{in}/mm	R_{out}/mm
1.2	1.0	640.0	700.0



(a) Three-dimensional model



(b) Computational domain

Figure 1. Schematic of RDC.

This article summarizes four common inlet structures based on [27]. To obtain a stable global equivalent ratio, a mass flow inlet is selected. The mass flow setting is obtained based on the total intake air pressure under experimental conditions (0.5 Mpa). Four inlet structures were studied to investigate the effect of different inlet structures on mixing characteristic in combustor as shown in Figure 2. Air is injected axially in Structures 1 and 2, as for Structures 3 and 4, air is injected radially. This study aims to discuss the mixing process and flow field within combustor, besides the inlet structure size is micro compared with the combustor. Therefore, the flow field characteristic of CH₄ and air within inlet is neglected and the attention is focused on the combustor region.

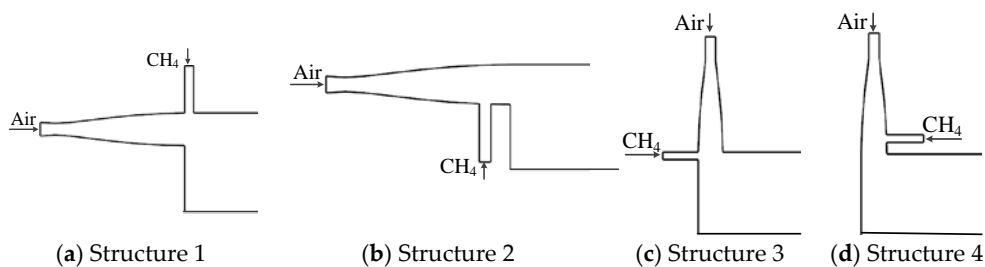


Figure 2. Schematic of different inlet structures.

2.2. Numerical Strategy

As shown in Figure 2, the injection direction of CH₄ and air keeps perpendicular in all structures and that is similar to the model of jets-in-crossflow. DeSpirito [28] and Chauvet et al. [29] proposed that the Spalart–Allmaras model achieves comparable results to experimental data in their study. Keimasi et al. [30] and Huang et al. [31] showed that the steady solver could get favorable agreement with experimental data for jet-in-crossflow simulation. Besides, Pudsey and Boyce [32] used the steady Reynolds-Averaged Navier Stokes (RANS) with Spalart–Allmaras model to investigate jet-in-crossflow model. Through integrated overall factors into account, based on ideal gas hypothesis, a steady RANS simulation with Spalart–Allmaras turbulence model is used in this study to explore the mixing characteristics of CH₄ and air in RDC by ANSYS Fluent. In this paper, a steady state solver based on density basis is used to solve the equation. The third order MUSCL (Monotone Upstream-Centered Schemes for Conservation Laws) reconfiguration scheme and AUSM (Advection Upstream Splitting Method) welcome style are used to discretize the convection term. To determine the accuracy of the model selected in this paper, the mixing process in [23] is simulated using the model selected in this paper, and the simulation results are compared with those in [23]. The comparison results are presented in Figure 3. According to the data in Figure 3, it can be found that the simulation value is close to the data in the literature, and the maximum error is only 3%, which proves the accuracy of the model selected in this paper.

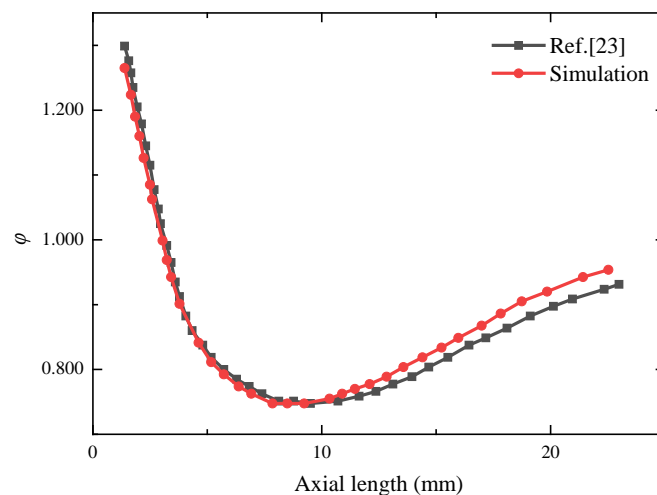


Figure 3. Comparison of simulated and literature values.

2.3. Boundary Conditions

The reactant is the stoichiometric mixture of CH₄ and air. The desired mass flow rate of CH₄ (\dot{m}_{CH_4}) and air (\dot{m}_{air}) is satisfied by mass flow inlet boundary condition applied to CH₄ and air inlets. Pressure on the outlet (p_b) is set by pressure outlet boundary condition. The inner wall, outer wall and inlet wall are all set as no slip adiabatic wall boundary. Specific parameters of boundaries are listed in Table 2, \dot{m}_{total} denotes the total mass flow rate in RDC, T_{total} denotes total temperature.

Table 2. Boundary condition parameters on various cases.

Case	$\dot{m}_{\text{CH}_4}/(\text{kg/s})$	$\dot{m}_{\text{air}}/(\text{kg/s})$	$\dot{m}_{\text{total}}/(\text{kg/s})$	$T_{\text{total}}/\text{K}$	p_b/MPa
1	0.7	12.01	12.71	300	0.1
2	0.5	8.58	9.08	300	0.1
3	0.1	1.72	1.82	300	0.1

2.4. Grid Independence Validation

When the meshing is completed, the value of Y^+ is in the range of 30–300, which meets the calculation requirements. Besides, the cfl number for the selected computational grid is 0.7, which also meets the calculation requirements. A grid independence validation is conducted to analyze the numerical results of four cases possessing different amount of grid numbers (2×10^5 , 2.3×10^5 , 2.6×10^5 , 3.3×10^5 , 2×10^6). Hexahedral meshes (shown in Figure 4) are generated by using ANSYS ICEM to discretize the computational domain. To compare the calculated results produced by various grid numbers computational domains, the mass fraction of CH_4 on the combustor outlet is selected to be the metric quantifying parameter. Figure 5 shows the distributions of CH_4 mass fraction along the outlet for every grid type. When the total amount of mesh is 2×10^5 and 2×10^6 , the distribution of CH_4 is already quite different from that of the other three kinds of grid total. There is less than 0.015% relative deviation between the medium grid sized domain (2.6×10^5) and fine grid sized domain (3.3×10^5), which means that the medium grid sized domain (2.6×10^5) is enough to produce analogous results compared to the fine sized domain.

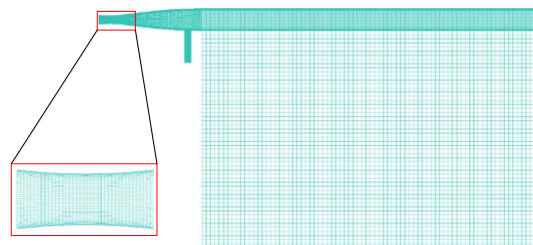


Figure 4. Grid of computational domain.

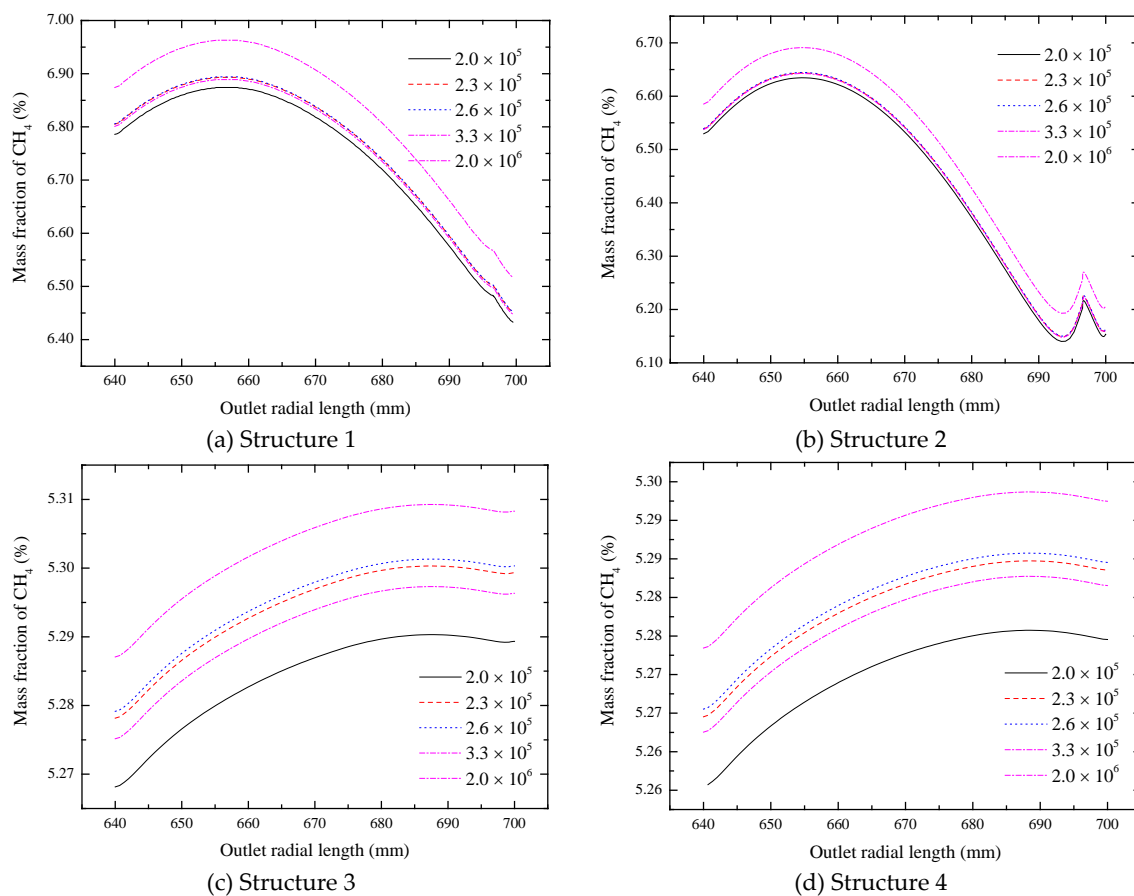


Figure 5. CH_4 distribution on the outlet.

3. Results and Discussions

To investigate the mixing of CH₄ and air in combustor, this paper first compares the mixing characteristics of different inlet structures. Then, the total pressure loss of each inlet structure is calculated. Finally, the ignition energy under the same equivalence ratio condition is calculated to determine the injection strategy of CH₄ and air.

3.1. Effects of Inlet Structure on Mixing Characteristics

Figure 6 shows the equivalence ratio contours of various inlet structures within the combustor region. According to the different equivalence ratio distributions, it can be found that the inlet structure of RDC influences the mixing characteristic of CH₄ and air obviously under various mass flow rates. The equivalence ratio is around 1 all over the combustor in Cases 1 and 2 comparatively except for Structures 1 and 2 in Case 3 (higher than 1). To gain a deep understanding of the mixing characteristics in the combustor, the parameter of unmixedness (s) is employed here to reflect the mixing quality of reactant, which is defined as the following [33]:

$$s = \frac{Y_{max} - Y_{ave}}{Y_{max}} \quad (1)$$

where Y_{max} is the maximal mass fraction of CH₄ on the planes perpendicular to x axis, Y_{ave} is the average mass fraction of CH₄ on the same plane. Lower s indicates higher uniformity.

A clear comparison of unmixedness variations under different inlet structures with axial length of combustor are displayed in Figure 7. The unmixedness drops monotonically with the increase of axial length, which indicates the mixing degree of CH₄ and air is gradually uniform. In the initial stage where CH₄ and air begin to interact with each other near the entrance of combustor, unmixedness drops rapidly compared to the following stage of slow decrease when close to outlet. A certain sequence of s is observed in Figure 7 when axial location is over 200 mm, Structure 3 < Structure 4 < Structure 1 < Structure 2, meaning Structure 3 has superior mixing quality and Structure 2 has poor mixing quality. Please note that unmixedness approaches to the same value and the difference of s almost disappears when the reactant close to the combustor outlet. Besides, as the total mass flow rate decreases (from Case 1 to 3), unmixedness rises up at the same axial location for every case. Large total mass flow rate in Case 1 produces higher inlet velocity of reactants. This causes excellent penetration ability of gas flow compared to the rest cases, which makes the violent interactions between CH₄ and air, the mixing quality is also enhanced correspondingly.

Figure 8 shows the stream lines and stream function contours of different inlet structures. To display the whole recirculation zone of each case, the axial length is extended to 600 mm in Figure 8. Based on the stream lines within combustor, the flow of reactant presents different trend when air axially or radially injected. As the air stream axially enters into the combustor, it keeps the axial direction all the time and exit straightly. When the air radially injected into the combustor, it flows along the inlet wall firstly and turns suddenly towards axial direction when encountering the corner of inner wall and inlet wall. This sudden change of flow direction might cause more drastic interaction of CH₄ and air compared to air axial injection scheme.

The recirculation zone appears in every case based on the distribution of stream lines, but the shape of them possesses slight difference for various structures. According to the theory quality of stream function, the volume flow rate of fluid passing through arbitrary curve (unit thickness) of two stream lines is equal to the difference of the two stream functions corresponding to the two stream lines. This means the difference of the stream lines is greater, larger reactant will flow past between them. For air axial injection (Structures 1 and 2), the maximal difference of stream function is observed at the zone close to the outer wall indicating the majority of reactant flow through this passage. Unlike air axial injection, for air radial injection (Structures 3 and 4), the maximal difference of stream function occurs at the region near the inlet and inner wall. That demonstrates most of the reactant passes through the

way where gas flows along the inlet wall and turns direction towards inner wall. Compared with the stream path of the majority of reactant in two air injection schemes, we can find that the stream path of air radial injection is longer than air axial injection, resulting in the stream interacts with recirculation zone sufficiently and efficiently for air radical injection. This can enhance the mixing quality of reactant to some extent.

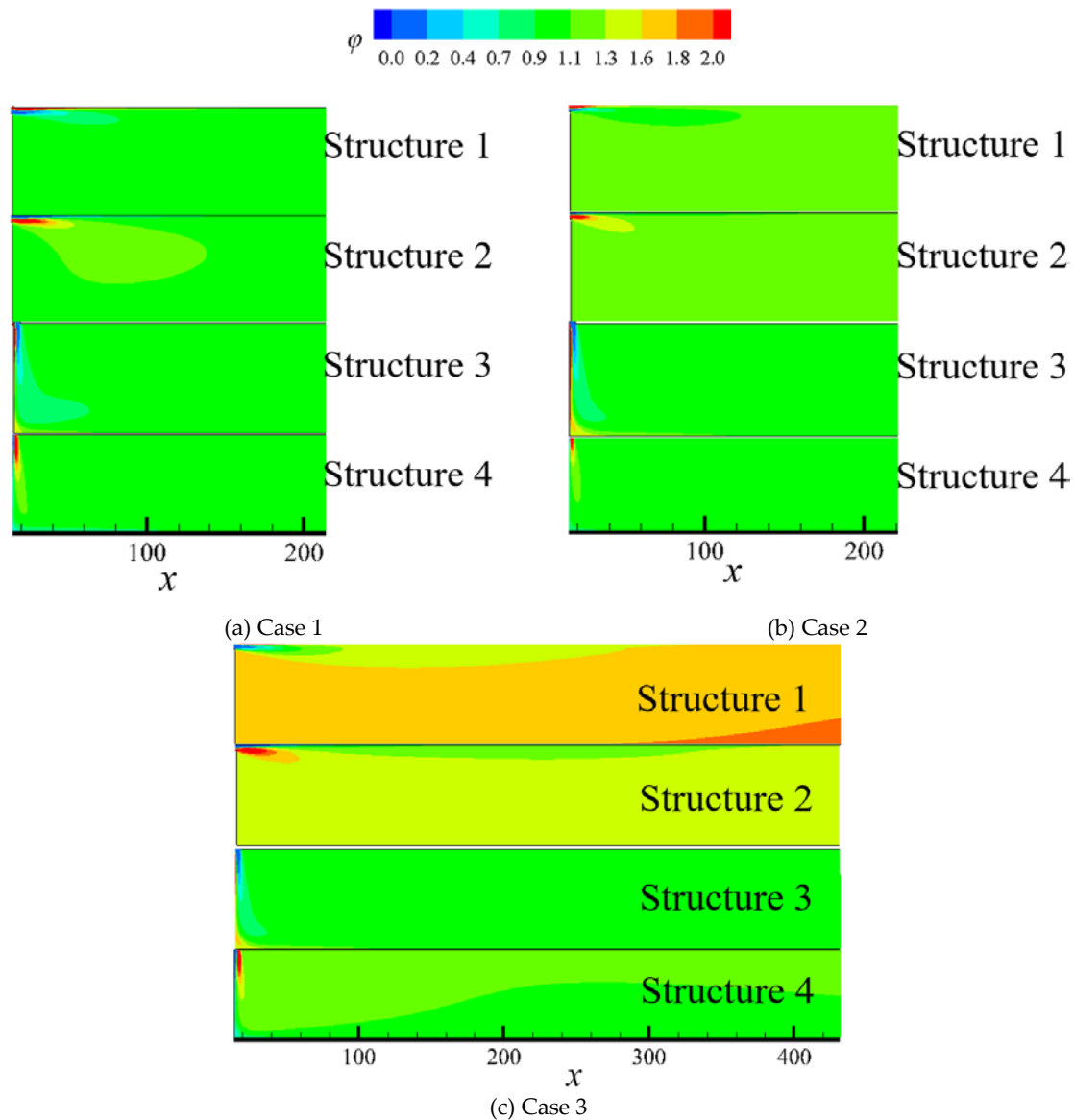


Figure 6. Contours of equivalence ratio for various inlet structures.

To understand the overall mixing characteristics of CH₄ and air in the combustor, the turbulent CH₄ mass diffusion is calculated here and the formula is defined as following where G_{CH₄} is the mass flux of CH₄, μ_t is the turbulent viscosity. Assuming gas momentum diffusivity is equal to species diffusivity, then, Schmidt number S_{ct} is a constant given by 0.7. Y_{CH₄} is the mass fraction of CH₄ [22].

$$M_{diff,CH_4} = \frac{1}{G_{CH_4}} \frac{\mu_t}{S_{ct}} \left[\left(\frac{\partial Y_{CH_4}}{\partial x} \right)^2 + \left(\frac{\partial Y_{CH_4}}{\partial y} \right)^2 \right]^{0.5} \quad (2)$$

The contours of turbulent CH₄ mass diffusion are shown in Figure 9. Diffusion peak of CH₄ is observed close to inlet region due to the first interaction of CH₄ and air. Besides, the diffusion

length of CH₄ is the longest in Structure 2 among all of the structures even though the total mass flow rate is changed. This can be explained by the different diffusion pattern affected by the injecting direction of CH₄. Taking Case 1 as an example, two diffusion peaks are observed for air axial injection (Structures 1 and 2) as shown in Figure 9a. W₁ means the diffusion peak which is close to outer wall and R means radial diffusion peak. The diffusivity of peak W₁ is restricted by outer wall because it almost attaches to the outer wall and CH₄ fails to diffuse towards that direction. For inlet Structure 2, CH₄ is injected towards the outer wall, making an army of CH₄ flow adjoin to the wall tightly. As a result, W₁ becomes the main diffusion peak in Structure 2. Recall that W₁ is limited by wall and the diffusivity of it probably cannot support the transport of such a quantity of CH₄, resulting in the CH₄ has to diffuse continuously downstream of the combustor in Structure 2. Therefore, Structure 2 has the longest diffusion length.

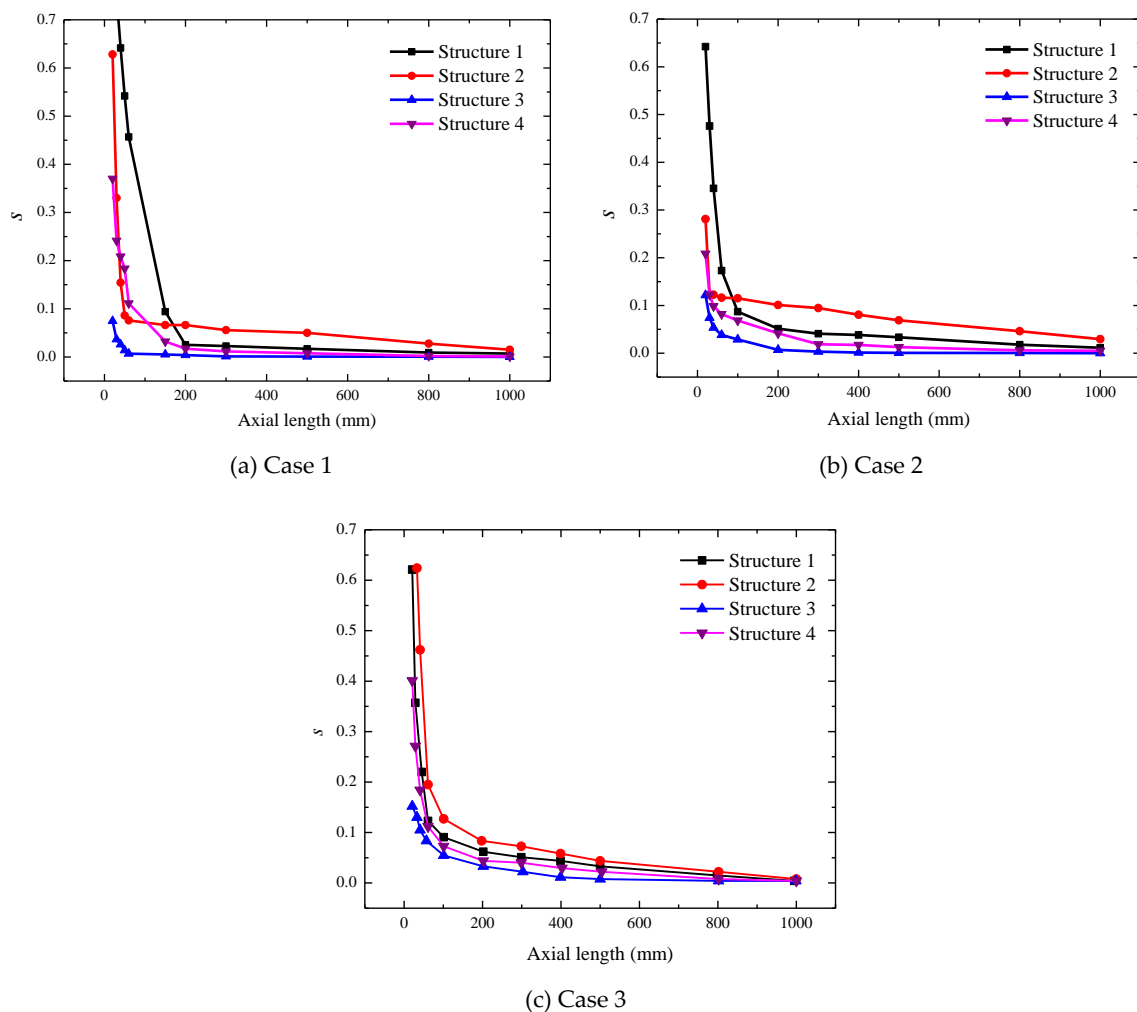


Figure 7. Effects of inlet structure on mixing non-uniformity.

Similarly, two diffusion peaks are also obtained for air radial injection scheme (Structures 3 and 4). One is close to inlet wall (W₂) diffusing radially towards inner wall and limited by inlet wall. After encountering inner wall, peak W₂ turns to diffuse axially and it is not restricted by inlet wall anymore. The other peak (A) diffuses axially towards the outlet of combustor and avoids being influenced by any wall. Therefore, two diffusion peaks both remain relatively high diffusion abilities, causing CH₄ diffuses faster compared to air radial injection.

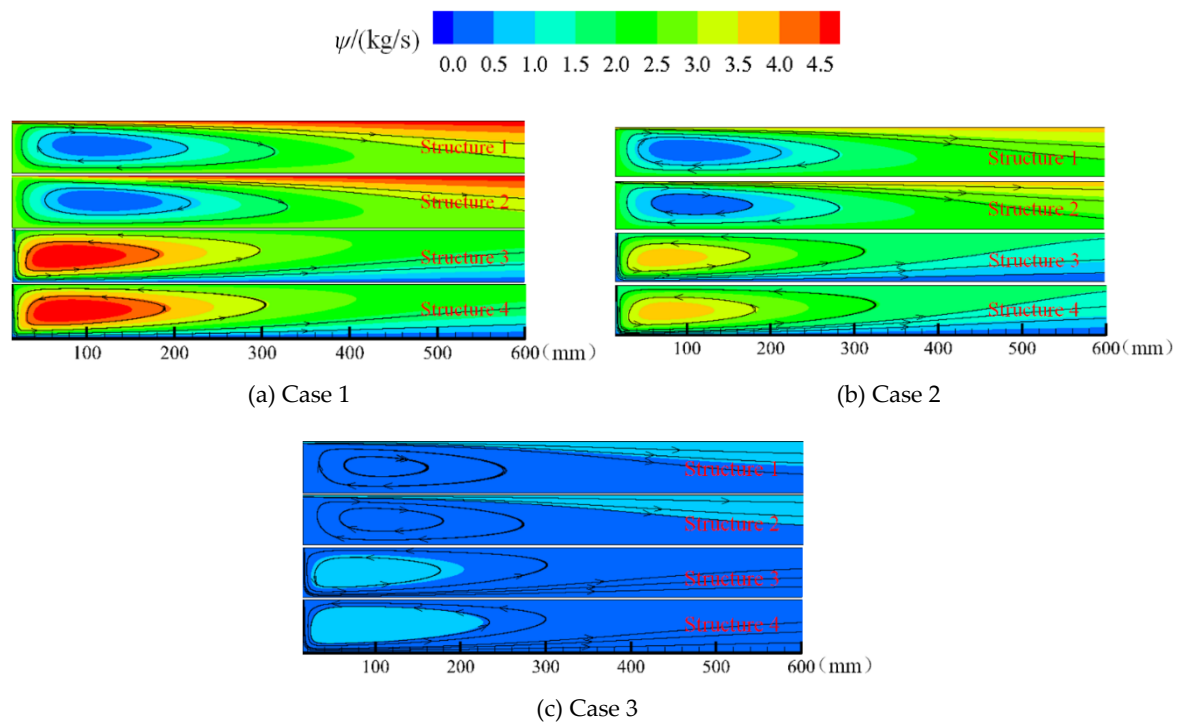


Figure 8. Effects of inlet structures on stream function and stream lines.

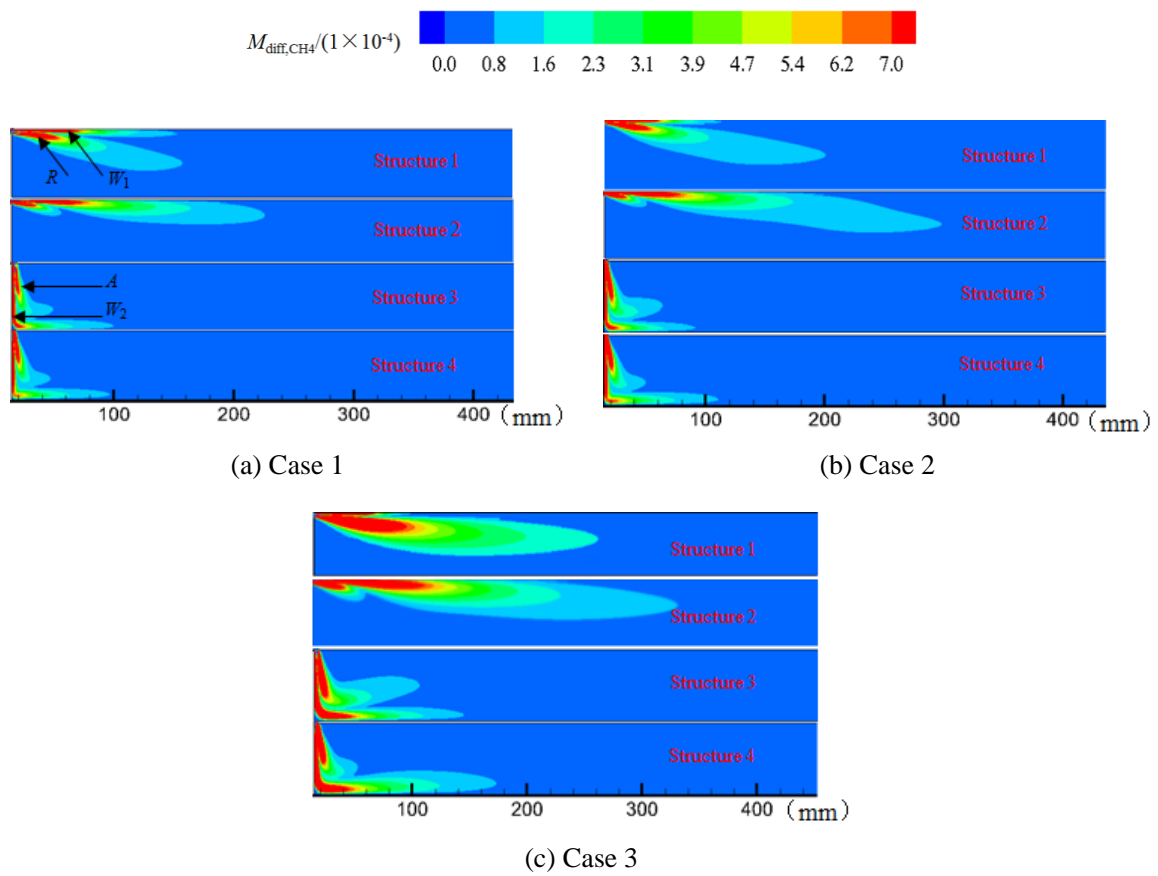


Figure 9. Contours of CH₄ mass diffusion.

3.2. Total Pressure Loss of Different Inlet Structures

Besides the mixing characteristic of reactant, the total pressure loss produced by mixing process is also a key aspect to be investigated thoroughly. Total pressure recovery parameter η_{rec} is defined as following where \bar{p}_t denotes the average total pressure on the plane perpendicular to x axis, $\bar{p}_{t,inj}$ is the average total pressure of reactant at the entrance of combustor, ρ is the density of reactant, $\bar{p}_{t,air}$ and \bar{p}_{t,CH_4} are average total pressure of air and CH_4 at the entrance of combustor respectively.

$$\eta_{rec} = \frac{\int \bar{p}_t \rho dS}{\bar{p}_{t,inj} \int \rho dS} \tag{3}$$

$$\bar{p}_{t,inj} = \frac{\dot{m}_{air} \bar{p}_{t,air} + \dot{m}_{CH_4} \bar{p}_{t,CH_4}}{\dot{m}_{air} + \dot{m}_{CH_4}} \tag{4}$$

Figure 10 displays the variations of total pressure recovery parameter with axial length of combustor. According to the trend of curves of all cases, η_{rec} drops monotonously with axial length increases. Please note that η_{rec} decreases rapidly at the head end of the combustor and major total pressure loss is produced here compared to the slight drop downstream. This can be explained by the turbulence intensity of the reactant due to the violent interaction between CH_4 and air when entering the combustor initially. To specify the turbulence characteristic of different regions within combustor, Figure 11 shows the contours of Reynolds number (Re). As expected, with the total mass flow rate decreases (from Case 1 to 3), the value of Re drops within the combustor. Re implies the interaction of CH_4 and air. Higher Re means more violent interactions of CH_4 and air.

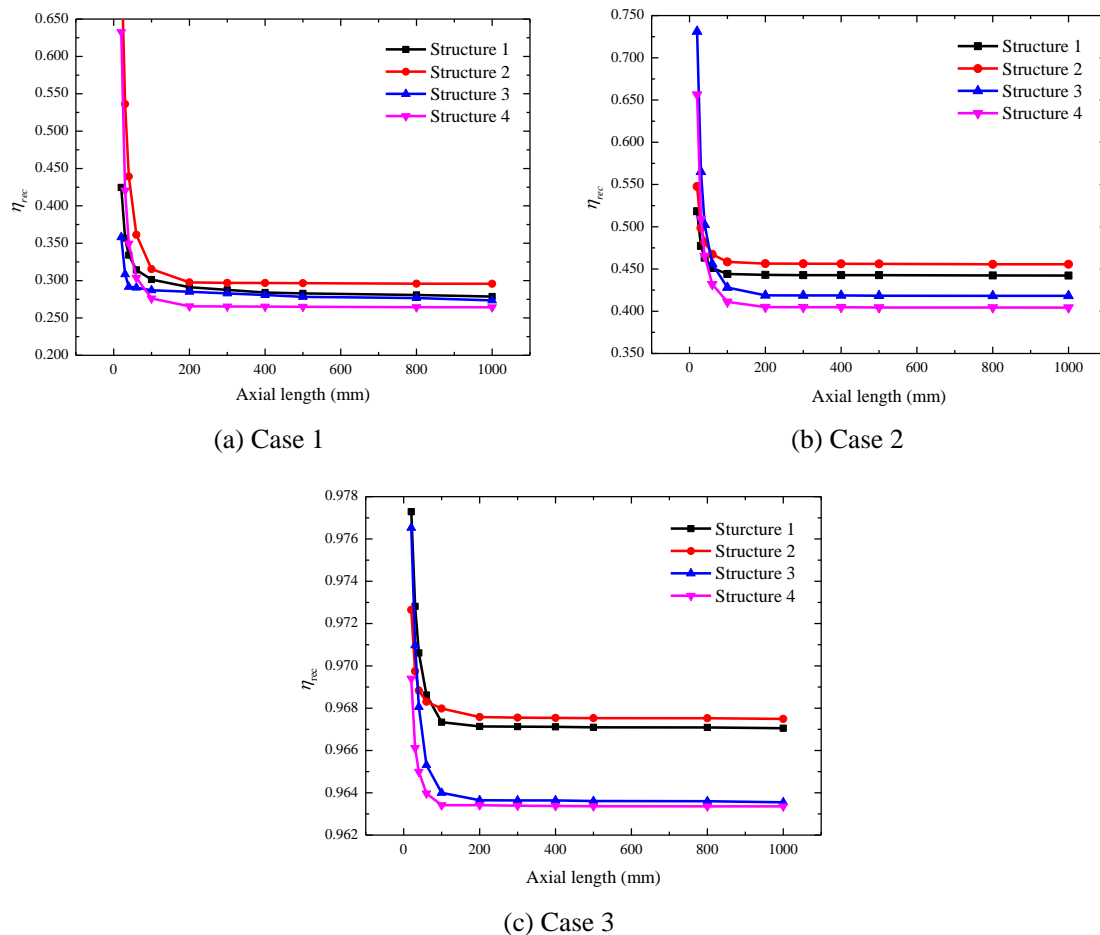


Figure 10. Total pressure recovery parameter distribution along axial direction.

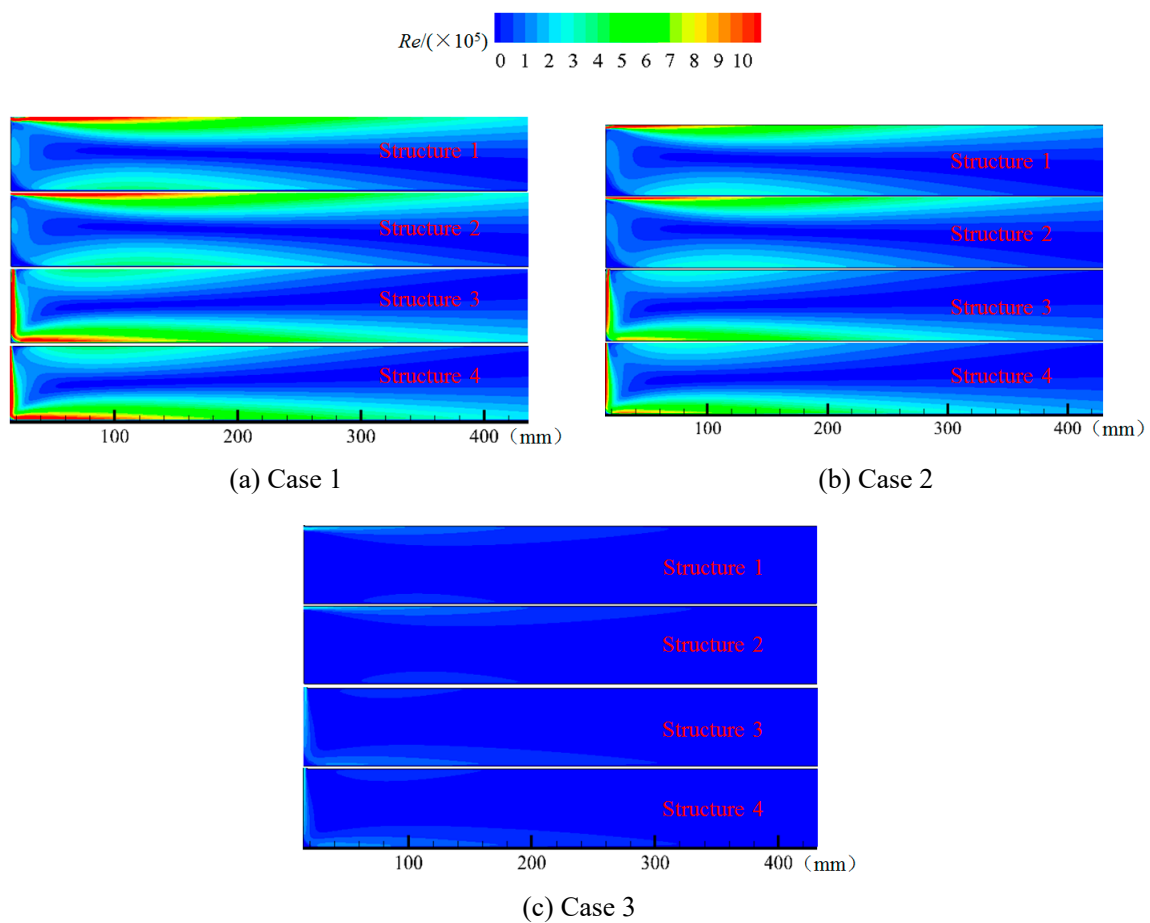


Figure 11. Contours of Reynolds number.

We can infer that larger mass flow rate of CH_4 and air might produce more total pressure loss because of the severer turbulent interaction of flow streams. The total pressure loss of each inlet structures is 28%, 32%, 27% and 26%, respectively in Case 1. Therefore, the value of η_{rec} is approximately 0.3 in Case 1, it arises to about 0.45 in Case 2 and reaches above 0.9 in Case 3. Even though the curves are interlaced each other at initial stage, a specific sequence of η_{rec} is observed after $x > 200$ mm, Structure 2 > Structure 1 > Structure 3 > Structure 4. This sequence is unchanged till the reactant flows to the outlet. This means air radial injections scheme produce lower total pressure compared to air axial injection due to its more violently turbulent flow of reactant when encountering the sharp corner of inlet and inner wall.

3.3. Effects of Inlet Structure on Critical Ignition Energy

The schematic of ignition position in combustor is displayed in Figure 12. In general, the pre-detonation tube is tangentially connected to the outer wall of RDC to provide ignition tangential kernel. Because the mixing quality and total pressure has little change after $x = 200$ mm, the point P (200 mm, 680 mm) close to outer wall is selected as the ignition position from which the tangential kernel is released by pre-detonation tube. To predict the critical ignition energy at point P, Formula (5), which was proposed by Wolanski [34], is employed, and it is defined as the following where E represents energy necessary to initiate a detonation, ρ_0 represents initial density, C_0 represents speed of sound in the combustible mixture, k_i represents coefficients for planar, cylindrical and spherical

cases. The static pressure and equivalence ratio at point P are listed in Table 3. Table 4 shows the critical ignition energy at point P.

$$R_{oc} = [E_i / (k_i \cdot \rho_0 \cdot C_0^2)]^{(1/i)} \quad (5)$$

Unexpectedly, according to the numerical results in Table 4, there is little difference for the pressure of ignition position in the same case. Therefore, the critical ignition energy is mainly dependent on the equivalence ratio at the ignition position, which essentially based on the mixing quality of reactant.

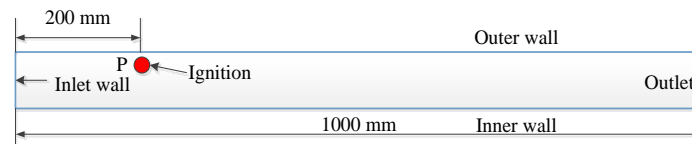


Figure 12. Schematic of ignition location.

Table 3. Static pressure (MPa)/ equivalence ratio in ignition position.

	Structure 1	Structure 2	Structure 3	Structure 4
Case 1	0.094/1.06	0.096/1.07	0.093/0.96	0.091/0.96
Case 2	0.097/1.14	0.097/1.20	0.096/1.01	0.095/1.04
Case 3	0.101/1.55	0.101/1.58	0.100/1.03	0.100/1.11

Table 4. Critical ignition energy (MJ) in ignition position.

	Structure 1	Structure 2	Structure 3	Structure 4
Case 1	2.859	2.866	2.846	2.861
Case 2	2.752	2.798	2.715	2.724
Case 3	3.248	3.412	2.728	2.732

The equivalence ratio of each structure is all close to 1 in Case 1, resulting in the critical ignition energy is almost at the same accordingly. As the total mass flow rate decreases in Cases 2 and 3, the equivalence ratio of air axial injection (Structures 1 and 2) is far away from optimal mixing value gradually compared to the air radial injection (Structures 3 and 4) which still keeps favorable mixing quality. As a result, the critical ignition energy of air axial injection become higher than air radial injection (i.e., the critical ignition energy of Structure 2 is 1.3 times than Structure 3 in Case 3). Please note that the ignition of Structure 2 is always the highest among all the structures, while Structure 3 is the lowest.

4. Conclusions

A mixing process of CH₄ and air in RDC is simulated accompanied with the evaluation of mixing quality and total pressure loss evaluation under different inlet structures. According to the numerical results, inlet structure has significant effect on the mixing characteristic, total pressure loss of the reactant and critical ignition energy. The primary conclusions from this work include the following:

- (1) The initial mixing process of reactant is very quick in a relative short distance at the head end of combustor owing to the first interaction of CH₄ and air. Compared to initial stage, the mixing process gradually slow down downstream. Because the majority of reactant interacts sufficiently with recirculation zone when air radial injection, so air radial injection scheme possesses superior mixing quality to air axial injection scheme. Based on mixing quality to identify the sequence of various structures, Structure 3 > Structure 4 > Structure 1 > Structure 2.
- (2) Within the scope of air axial injection scheme, the structure of CH₄ injecting towards outer wall has the longest mixing length due to the main diffusion peak is restricted by the outer wall, which limits the ability of CH₄ diffusion.

- (3) As the mass flow rate increase, the total pressure loss of reactant in combustor increases correspondingly owing to violently turbulent intensity. When the total mass flow rate is 12.71 kg/s, total pressure recovery parameter is around 0.3. As the total mass flow rate decrease to 1.82 kg/s, total pressure recovery parameter rises to above 0.96.
- (4) At the ignition position in our study, pressure has little effect on the critical ignition energy. The equivalence ratio determines the critical ignition energy, meaning mixing quality plays a crucial role for the ignition process. Comparing four inlet structures, Structure 2 needs the highest critical ignition energy. Owing to the superior mixing quality of Structure 3, its critical ignition energy is the lowest.

Author Contributions: Conceptualization, Z.L.; methodology, S.J.; software and validation, Q.M.; investigation, S.J. and N.Z.; writing—original draft preparation, S.J. and H.Z.; writing—review and editing, N.Z. and J.Y. All authors have read and agreed to the published version of the manuscript.

Funding: This research was funded by the National Nature Science Foundation of China (Grant No. 51709059), the Province Nature Science Foundation of Heilongjiang (Grant No. QC2017045) and the Fundamental Research Funds for the Central Universities (Grant No. HEUCFJ170304, Grant No. HEUCFP201719).

Conflicts of Interest: We declare that we have no conflict of interest.

References

1. Wolański, P. Detonative propulsion. *Proc. Combust. Inst.* **2013**, *34*, 125–158. [[CrossRef](#)]
2. Anand, V.; George, A.S.; Driscoll, R.; Gutmark, E. Characterization of instabilities in a rotating detonation combustor. *Int. J. Hydrog. Energy* **2015**, *40*, 16649–16659. [[CrossRef](#)]
3. Gobbato, P.; Masi, M.; Toffolo, A.; Lazzaretto, A. Calculation of the flow field and NO_x emissions of a gas turbine combustor by a coarse computational fluid dynamics model. *Energy* **2012**, *45*, 445–455. [[CrossRef](#)]
4. Schwer, D.A.; Kailasanath, K. Characterizing NO_x emissions for air-breathing rotating detonation engines. In Proceedings of the 52nd AIAA/SAE/ASEE Joint Propulsion Conference, Salt Lake, UT, USA, 25–27 July 2016. [[CrossRef](#)]
5. Kazhikathra, K.; Douglas, S. Exhaust Gas Emissions from a Rotating Detonation-wave Engine. In Proceedings of the 68th Annual Meeting of the APS Division of Fluid Dynamics, Boston, MA, USA, 22–24 November 2015.
6. Bennett, D.; Schneider, J.; Wilson, R.; Bienias, J.; Berrykravis, E.; Arnold, S. Rotating detonation engine operation. In Proceedings of the 50th AIAA Aerospace Sciences Meeting including the New Horizons Forum and Aerospace Exposition, Nashville, TN, USA, 09–12 January 2012.
7. Kindracki, J.; Kobiera, A.; Wolański, P.; Gut, Z.; Folsiak, M.; Swiderski, K. Experimental and numerical study of the rotating detonation engine in hydrogen-air mixtures. *Prog. Propuls. Phys.* **2011**, *2*, 663–670.
8. Shank, J.; King, P.; Karnesky, J.; Schauer, F.; Hoke, J. Development and testing of a modular rotating detonation engine. In Proceedings of the 50th AIAA Aerospace Sciences Meeting including the New Horizons Forum and Aerospace Exposition, Nashville, TN, USA, 9–12 January 2012.
9. Bussing, T.; Pappas, G. An introduction to pulse detonation engines. In Proceedings of the 32nd Aerospace Sciences Meeting and Exhibit, Reno, NV, USA, 10–13 January 1994.
10. Kailasanath, K. Recent developments in the research on pulse detonation engines. *AIAA J.* **2011**, *41*, 145–159. [[CrossRef](#)]
11. Wintenberger, E.; Shepherd, J.E. Model for the performance of airbreathing pulse-detonation engines. *J. Propuls. Power.* **2006**, *22*, 593–603. [[CrossRef](#)]
12. Ostrander, M.; Hyde, J.; Young, M.; Kissinger, R.; Pratt, D. Standing oblique detonation wave engine performance. In Proceedings of the 23rd Joint Propulsion Conference, San Diego, CA, USA, 29–02 July 1987.
13. Fusina, G.; Sislian, J.P.; Parent, B. Formation and stability of near Chapman–Jouguet standing oblique detonation waves. *AIAA J.* **2005**, *43*, 1591–1604. [[CrossRef](#)]
14. Schwer, D.; Kailasanath, K. Feedback into mixture plenums in rotating detonation engines. In Proceedings of the 50th AIAA Aerospace Sciences Meeting including the New Horizons Forum and Aerospace Exposition, Nashville, TN, USA, 9–12 January 2012.

15. Fotia, M.; Hoke, J.; Schauer, F. Propellant plenum dynamics in a two-dimensional rotating detonation experiment. In Proceedings of the 52nd Aerospace Sciences Meeting, National Harbor, MD, USA, 13–17 January 2014.
16. Wu, D.; Liu, Y.; Liu, Y.; Wang, J. Numerical investigations of the restabilization of hydrogen–air rotating detonation engines. *Int. J. Hydrog. Energy*. **2014**, *39*, 15803–15809. [[CrossRef](#)]
17. Shao, Y.; Wang, J. Change in continuous detonation wave propagation mode from rotation detonation to standing detonation. *Chin. Phys. Lett.* **2010**, *27*. [[CrossRef](#)]
18. Frolov, S.M.; Dubrovskii, A.V.; Ivanov, V.S. Three-dimensional numerical simulation of the operation of a rotating-detonation chamber with separate supply of fuel and oxidizer. *Russ. J. Phys. Chem.* **2013**, *7*, 35–43. [[CrossRef](#)]
19. Bykovskii, F.A.; Zhdan, S.A.; Vedernikov, E.F. Continuous spin detonation of fuel-air mixtures. *Combust. Explos. Shock Waves*. **2006**, *42*, 463–471. [[CrossRef](#)]
20. Stoddard, W.A.; George, A.S.; Driscoll, R. Computational analysis of existing and altered rotating detonation engine inlet designs. In Proceedings of the 50th AIAA/ASME/SAE/ASEE Joint Propulsion Conference, Cleveland, OH, USA, 28–30 July 2014.
21. Stoddard, W.; Gutmark, E. Comparative numerical study of RDE injection designs. In Proceedings of the 52nd AIAA Aerospace sciences meeting, National Harbor, MD, USA, 13–17 January 2014.
22. Driscoll, R.; George, A.; Anand, V. Numerical investigation of inlet injection in a rotating detonation engine. In Proceedings of the 53rd AIAA Aerospace Sciences Meeting, Kissimmee, FL, USA, 5–9 January 2015.
23. Driscoll, R.; Aghasi, P.; George, A.S.; Gutmark, E.J. Three-dimensional, numerical investigation of reactant injection variation in a H₂/air rotating detonation engine. *Int. J. Hydrog. Energy*. **2016**, *41*, 5162–5175. [[CrossRef](#)]
24. Gaillard, T.; Davidenko, D.; Dupoirieux, F. Numerical optimisation in non-reacting conditions of the injector geometry for a continuous detonation wave rocket engine. *Acta Astronaut.* **2015**, *111*, 334–344. [[CrossRef](#)]
25. Andrus, I.Q.; King, P.; Polanka, M.D.; Schauer, F.; Hoke, J. Experimentation of a premixed rotating detonation engine utilizing a variable slot feed plenum. In Proceedings of the 54th AIAA Aerospace Sciences Meeting, San Diego, CA, USA, 4–8 January 2016.
26. Andrus, I.Q.; King, P.; Polanka, M.D.; Schauer, F.; Hoke, J.L. Design of a premixed fuel-oxidizer system to prevent flashback in a rotating detonation engine. In Proceedings of the 54th AIAA Aerospace Sciences Meeting, San Diego, CA, USA, 4–8 January 2016.
27. Rankin, B.A.; Fugger, C.A.; Richardson, D.R.; Cho, K.Y.; Hoke, J.; Caswell, A.W.; Gord, J.R.; Schauer, F. Evaluation of mixing processes in a non-premixed rotating detonation engine using acetone PLIF. In Proceedings of the 54th AIAA Aerospace Sciences Meeting, San Diego, CA, USA, 4–8 January 2016.
28. DeSpirito, J. Turbulence model effects on cold-gas lateral jet interaction in a supersonic crossflow. *J. Spacecr. Rocket.* **2015**, *52*, 836–852. [[CrossRef](#)]
29. Chauvet, N.; Deck, S.; Jacquin, L. Numerical study of mixing enhancement in a supersonic round jet. *AIAA J.* **2007**, *45*, 1675–1687. [[CrossRef](#)]
30. Keimasi, M.R.; Taeibi-Rahni, M. Numerical simulation of jets in a crossflow using different turbulence Models. *AIAA J.* **1971**, *39*, 2268–2277. [[CrossRef](#)]
31. Huang, W.; Liu, W.; Li, S.; Xia, Z.; Liu, J.; Wang, Z. Influences of the turbulence model and the slot width on the transverse slot injection flow field in supersonic flows. *Acta Astronaut.* **2012**, *73*, 1–9. [[CrossRef](#)]
32. Pudsey, A.S.; Boyce, R.R. Numerical investigation of transverse jets through multiport injector arrays in a supersonic crossflow. *J. Propuls. Power* **2010**, *26*, 1225–1236. [[CrossRef](#)]
33. Pan, G. Design and performance study of gas steam injection double fuel nozzle. Ph.D. Thesis, Harbin Engineering University, Harbin, China, 2015.
34. Wolański, P.; Kauffman, C.W.; Nicholls, J.A. Detonation of Methane–Air Mixtures. *Eighteenth Symp. Int. Combust.* **1980**, *18*, 1651–1660. [[CrossRef](#)]

